Available online at www.sciencedirect.com
ScienceDirect
Journal of Hazardous Materials 147 (2007) 581–587
Journal of Hazardous Materials
www.elsevier.com/locate/jhazmat

Synthesis, characterization and photocatalytic activity of mesoporous titania nanorod/titanate nanotube composites

Huogen Yu [a], Jiaguo Yu [a,*], Bei Cheng [a], Jun Lin [b]

[a] *State Key Laboratory of Advanced Technology for Material Synthesis and Processing, Wuhan University of Technology, Luoshi Road 122#, Wuhan 430070, PR China*
[b] *Department of Chemistry, Renmin University of China, Beijing 100872, PR China*

Received 14 December 2006; received in revised form 14 January 2007; accepted 15 January 2007
Available online 19 January 2007

Abstract

Mesoporous titania nanorod/titanate nanotube composites were prepared using TiF_4 and H_3BO_3 as the precursors. The prepared samples were characterized with TEM, SEM, XRD, HRTEM, and nitrogen adsorption–desorption isotherms. The photocatalytic activities were evaluated by photocatalytic oxidation of acetone in a gas phase and photocatalytic discolorization of methyl orange aqueous solution in an aqueous phase, respectively. The results indicated that the photocatalytic activity of the mesoporous titania nanorod/titanate nanotube composites exceeded that of P25 by a factor of about 2.5 times for the photocatalytic oxidation of acetone. This could be attributed to the fact that the former had a larger specific surface area and a higher pore volume. Moreover, the mesoporous titania nanorod/titanate nanotube composites, which could be readily separated after photocatalytic reaction in an aqueous phase, exhibited highly photocatalytic activity for the degradation of methyl orange aqueous solution.

Keywords: TiO_2; Titanate nanotubes; Nanorods; Photocatalytic activity; Composites; Mesoporous

1. Introduction

Heterogeneous photocatalysis, a new water and air purification technique, has attracted great attention in the past decade [1–6]. Among various oxide semiconductor photocatalysts, titania is a very important photocatalyst due to its biological and chemical inertness, strong oxidizing power, nontoxicity, and long-term stability against photo and chemical corrosion [1–6]. Despite its great potential, the low photocatalytic efficiency of TiO_2 hinders the commercialization of photocatalytic oxidation technology [7]. Therefore, the further improvement of photoactivity of TiO_2 is one of the most important tasks from the point of view of practical use. To achieve this purpose, mesoporous TiO_2 has attracted much attention due to its large surface area and high pore volume [8–10]. Usually, mesoporous TiO_2 materials are synthesized through conventional approaches using various surfactants as templates. However, the obtained samples require the removal of these templates by calcination or extraction to obtain the final products. The calcination at high temperature may cause the collapse of the framework of mesoporous materials, and the extraction is time-consuming. On the other hand, when TiO_2 powder is used as a photocatalyst for water purification, it shows highly photocatalytic activity due to its large surface area. However, conventional powdered photocatalysts have a serious limitation—the need for post-treatment separation in a slurry system after photocatalytic reaction. Though this can be overcome by immobilizing TiO_2 particles as thin films on solid substrates [3,11–13], the formation of TiO_2 films on the substrates significantly reduced the specific surface area of TiO_2 photocatalysts, resulting in a decrease of photocatalytic activity. Therefore, it is necessary to develop novel synthesis approach to prepare mesoporous TiO_2 photocatalysts, which not only has highly photocatalytic activity, but also can be steadily separated after photocatalytic reaction.

Recently, titanate nanotubes with large specific surface area, and high pore volume have appeared to be a promising, and important prospect due to their fascinating microstructures, and promising photo-electrochemical applications since the innovative work was reported by Kasuga et al. [14–19]. Using a simple

* Corresponding author. Tel.: +86 27 87871029; fax: +86 27 87879468.
E-mail addresses: jiaguoyu@yahoo.com (J. Yu), jlin@chem.ruc.edu.cn (J. Lin).

0304-3894/$ – see front matter © 2007 Elsevier B.V. All rights reserved.
doi:10.1016/j.jhazmat.2007.01.054

hydrothermal treatment of crystalline TiO_2 particles with NaOH aqueous solutions, high-quality nanotubes with uniform diameter of around 10 nm were obtained and their specific surface area reached more than 400.0 m^2/g [14,15]. Unfortunately, the nanotubes prepared by this hydrothermal method showed almost no photocatalytic activity for the photocatalytic degradation of acetone in our experiment. Following the pioneering works, the obtained nanotubes were actually not TiO_2, but might be hydrogen titanate [17,20]. According to our previous study, the anatase TiO_2 particles coated on the surface of the glass fibers showed a higher photocatalytic activity, and a lower deactivation rate compared with the TiO_2 films [6]. Considering the large specific surface area, high pore volume, and one-dimensional structure of the titanate nanotubes, it is expected that the combination of anatase TiO_2 nanoparticles or nanorods and the titanate nanotubes would endow titania with unique properties and multiple functions. Therefore, it is worthwhile to explore the synthesis of mesoporous titania nanorod/titanate nanotube composites and their corresponding photocatalytic activities.

In the present work, titanate nanotubes were first prepared by a hydrothermal reaction using a 10 M NaOH aqueous solution and Degussa P25 as precursors. Subsequently, the as-prepared nanotubes were dipped into the mixed solutions of TiF_4 and H_3BO_3 to obtain the mesoporous titania nanorod/titanate nanotube composites. The photocatalytic activities of the obtained samples were evaluated by photocatalytic oxidation of acetone in a gas phase and photocatalytic discolorization of methyl orange aqueous solution in an aqueous phase, respectively.

2. Experimental

2.1. Preparation of titanate nanotubes

Titanate nanotubes were prepared using a chemical process similar to that described by Kasuga et al. [14,15]. TiO_2 source used for the titanate nanotubes was commercial-grade TiO_2 powder (P25, Degussa AG, Germany) with crystalline structure of ca. 20% rutile and ca. 80% anatase and primary particle size of ca. 30 nm. In a typical nanotube preparation, 1.5 g of the TiO_2 powder was mixed with 140 ml of 10 M NaOH solution followed by hydrothermal treatment of the mixture at 150 °C in a 200 ml Teflon-lined autoclave for 48 h. After hydrothermal reaction, the precipitate was separated by filtration and washed with a 0.1 M HCl solution and distilled water until the pH value of the rinsing solution reached ca. 6.5, approaching the pH value of the distilled water. The washed samples were dried in a vacuum oven at 80 °C for 8 h.

2.2. Preparation of the mesoporous titania nanorod/titanate nanotube composites

TiF_4 and H_3BO_3 were used as the precursors for the preparation of mesoporous titania nanorod/titanate nanotube composites. In a typical synthesis, TiF_4 and H_3BO_3 were dissolved in distillated water, respectively. Then, the as-prepared aqueous solutions of TiF_4 and H_3BO_3 were mixed, stirred, and used as the reaction solution. The resultant precursor concentrations of the reaction solution were 0.025 M for TiF_4 and 0.075 M for H_3BO_3. Subsequently, 0.1 g of the washed titanate nanotubes were added into 100 ml of the reaction solution and then maintained at 60 °C for 12 h. After the reactions, the samples were filtered, rinsed with distilled water and dried in a vacuum oven at 60 °C for 8 h. For comparison, the reaction solution of TiF_4 and H_3BO_3 in the absence of titanate nanotubes was mixed and kept at 60 °C for 12 h to obtain the TiO_2 spherical aggregates.

2.3. Characterization

Morphology observation was performed on a JSM-5610LV scanning electron microscope (SEM, JEOL, Japan). X-ray diffraction (XRD) patterns were obtained on a D/MAX-RB X-ray diffractometer (Rigaku, Japan), using Cu Kα irradiation at a scan rate (2θ) of 0.05° s^{-1} and were used to determine the phase structure of the obtained samples. The accelerating voltage and the applied current were 15 kV and 20 mA, respectively. Transmission electron microscopy (TEM) analysis were conducted with a JEM-2010F electron microscope (JEOL, Japan), using 200 kV accelerating voltage. Nitrogen adsorption–desorption isotherms were obtained on an ASAP 2020 (Micromeritics Instruments, USA) nitrogen adsorption apparatus. All the samples were degassed at 100 °C prior to BET measurements. The Brunauer–Emmett–Teller (BET) specific surface area (S_{BET}) was determined by a multipoint BET method using the adsorption data in the relative pressure (P/P_0) range of 0.05–0.25. Desorption isotherm was used to determine the pore size distribution using the Barret–Joyner–Halender (BJH) method [21]. The nitrogen adsorption volume at the relative pressure (P/P_0) of 0.970 was used to determine the pore volume and the average pore size.

2.4. Photocatalytic oxidation of acetone in a gas phase

Acetone, formaldehyde and other volatile organic compounds (VOCs) are common indoor air pollutants in modern houses, which have been the subject of numerous complaints regarding health disorders, such as leukemia, nausea, headache and fatigue. Therefore, we chose acetone (CH_3COCH_3) as a model contaminate chemical. Photocatalytic oxidation of acetone is based on the following reaction [22–24]:

$$CH_3COCH_3 + 4O_2 \rightarrow 3CO_2 + 3H_2O \quad (1)$$

The measurement of photocatalytic activities of the prepared samples was performed in a 15 L reaction reactor using the photodegradation of acetone with an initial concentration of 350 ± 20 ppm. The photocatalysts were prepared by coating an aqueous suspension of powder samples onto three dishes with a diameter of ca. 7.0 cm. The dishes containing catalysts were dried at 100 °C, and then cooled to room temperature before being used. The weight of the catalysts used for each experiment was kept at ca. 0.5 g. After the catalysts were placed in the reactor, a small amount of acetone was injected with a syringe into the reactor. The reactor was connected to a $CaCl_2$-containing

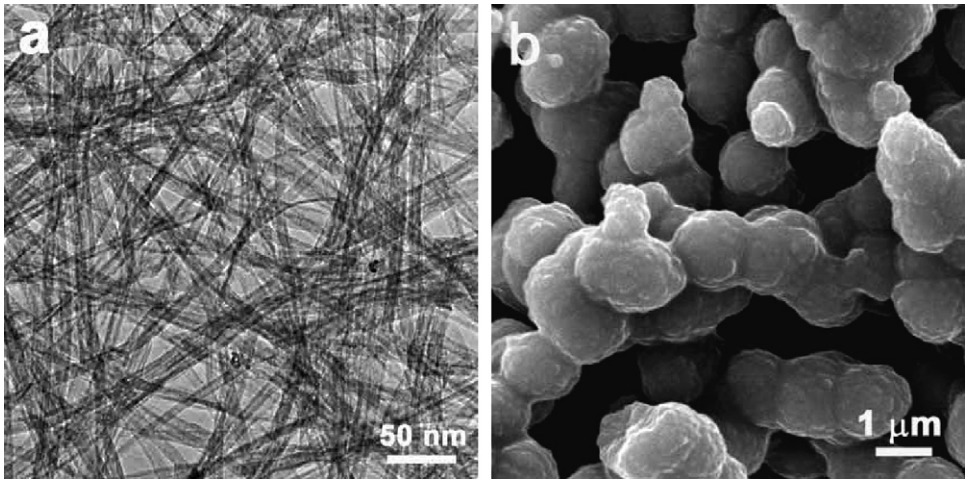

Fig. 1. (a) TEM image of the as-prepared titanate nanotubes; (b) SEM image of the TiO_2 spherical aggregates obtained in the absence of titanate nanotubes.

dryer used for controlling the initial humidity in the reactor. The acetone vapor was allowed to reach adsorption–desorption equilibrium with catalysts in the reactor prior to UV light irradiation. Integrated UV intensity in the range of 310–400 nm striking the coatings, measured with a UV radiometer (Model: UV-A, made in Photoelectric Instrument Factory of Beijing Normal University), was 2.5 mW/cm^2, while the peak wavelength of UV light was 365 nm. The concentration analysis of acetone, carbon dioxide and water vapor in the reactor was conducted on line with a Photoacoustic IR Multigas Monitor (INNOVA Air Tech Instruments Model 1312). The photocatalytic activity of the catalyst samples can be quantitatively evaluated by comparing the apparent reaction rate constants. The photocatalytic oxidation of acetone is a pseudo-first-order reaction and its kinetics may be expressed as follows: $\ln(C_0/C) = kt$ [23], where k is the apparent reaction rate constant, C_0 and C are the initial concentration and the reaction concentration of acetone, respectively.

2.5. Photocatalytic discolorization of methyl orange in an aqueous phase

The evaluation of photocatalytic activity of the prepared samples for the photocatalytic discolorization of methyl orange aqueous solution was performed at ambient temperature. Experimental process was as follows: the prepared samples (0.02 g) were dispersed in a 25 mL methyl orange aqueous solution with a concentration of 3.1×10^{-5} mol L^{-1} in a rectangular cell ($52W \times 155L \times 30H$ mm). A 15-W 365 nm UV lamp (Cole-Parmer Instrument Co.) was used as a light source. The average light intensity striking on the surface of the reaction solution was about 112 μW cm^{-2}, as measured by a UV meter (made in the photoelectric instrument factory of Beijing normal university) with the peak intensity of 365 nm. The concentration of methyl orange was determined by an UV–vis spectrophotometer (UV-2550, Shimadzu, Japan). After UV irradiation for some time, the reaction solution was filtrated to measure the concentration change of methyl orange.

3. Results and discussion

3.1. Morphology and phase structure of the titanate nanotubes and the mesoporous titania nanorod/titanate nanotube composites

Fig. 1(a) shows TEM image of the as-prepared titanate nanotubes obtained by a hydrothermal reaction using Degussa P25 and 10 M NaOH aqueous solution as the precursors at 150 °C for 48 h. A large amount of nanotubes with diameters of 7–12 nm and lengths of several hundreds nanometers are obtained. Further observation indicates that the prepared nanotubes possess uniform inner and outer diameters along their length, in good agreement with the previous reports [16,17]. The corresponding XRD pattern of the obtained nanotubes (Fig. 2(a)) indicates that the crystal structure of the resulted nanotubes is similar to that of $H_2Ti_3O_7$ ($Na_2Ti_3O_7$) [16,17], $Na_xH_{2-x}Ti_3O_7$ [20],

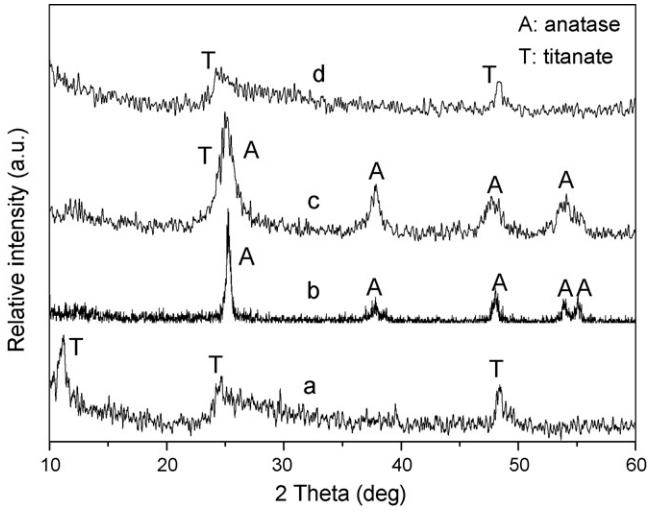

Fig. 2. XRD patterns of: (a) the as-prepared titanate nanotubes; (b) the TiO_2 spherical aggregates obtained in the absence of titanate nanotubes; (c) the mesoporous titania nanorod/titanate nanotube composites; (d) the treated titanate nanotubes in distilled water at 60 °C.

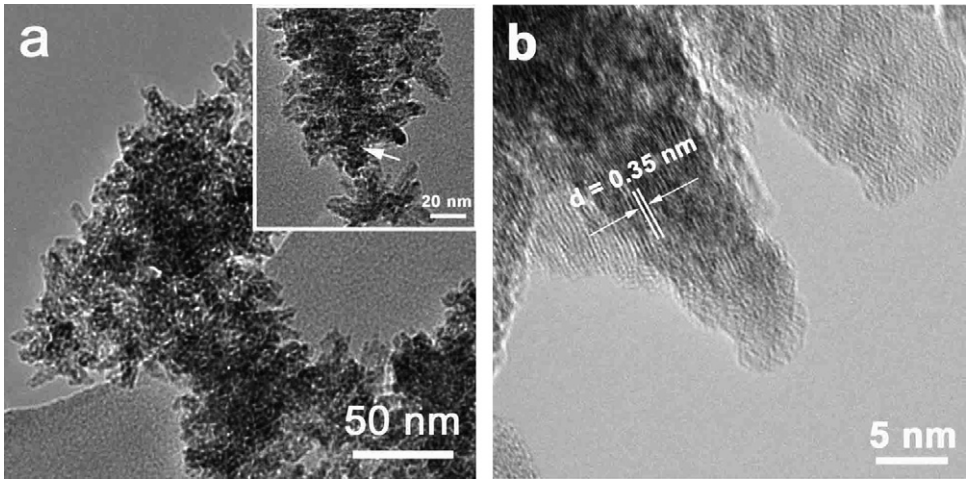

Fig. 3. (a) TEM image of nanorod/titanate nanotube composites and high-magnification TEM image (inset in a), and (b) HRTEM image of the TiO_2 nanorods.

$H_xTi_{2-x/4}\square_{x/4}O_4$ ($x = 0.75$) [25], probably due to their similar layered titanate family. Similar phase structure was also found in the titinate nanoribbons reported in our previous study [26]. EDX analysis clearly demonstrated the absence of sodium ions in the obtained nanotubes (not shown here). Therefore, the sodium ions were substituted completely by protons after the nanotubes were washed with HCl aqueous solution and distilled water. Considering the absence of Na in the nanotubes, the obtained nanotubes may be described as $H_2Ti_nO_{2n+1}\cdot xH_2O$ and can be attributed to hydrogen titanate [27].

When the mixed solution of 0.025 M TiF_4 and 0.075 M H_3BO_3 was incubated at 60 °C for 12 h in the absence of titanate nanotubes, TiO_2 spherical aggregated particles with a size of 1–3 μm (Fig. 1(b)) were formed. The corresponding XRD pattern (Fig. 2(b)) indicated that the crystal structure of these aggregated particles was anatase phase. However, when the titanate nanotubes were added into the above mixed reaction, the TiO_2 nanorods were uniformly coated on the surface of the titanate nanotubes (Fig. 3(a)). Therefore, it was deduced that the TiO_2 nanorods on the surface of the titanate nanotubes were formed via a surface-promoted heterogeneous nucleation and growth mechanism. The diameters and lengths of the TiO_2 nanorods were 5–10 nm and 15–40 nm, respectively. Corresponding XRD pattern (Fig. 2(c)) exhibited obvious diffraction peaks of anatase TiO_2, suggesting that the obtained titania nanorod/titanate nanotube composites contained anatase phase. To clarify the formation of anatase phase in the Fig. 2(c), the as-prepared titanate nanotubes were dipped into the distilled water, and then kept at 60 °C for 12 h at the same conditions (without the addition of TiF_4 and H_3BO_3). The XRD pattern (Fig. 2(d)) exhibited no diffraction peaks of anatase TiO_2 in addition to the diffraction peaks of titanate. This indicates that the anatase phase in the Fig. 2(c) can be attributed to the TiO_2 nanorods coated on the surface of the titanate nanotubes. Though the nanotube-like structure cannot be clearly observed in the TEM image due to the coating of the TiO_2 nanorods, it can be clearly seen that the diameter corresponding to the nanotube has no obvious change after the formation of the titania nanorod/titanate nanotube composites, as indicated by arrow (Fig. 3(a), inset). A representative HRTEM lattice image of the TiO_2 nanorods coated on the surface of the titanate nanotubes is shown in Fig. 3(b). By measuring the lattice fringes, the resolved inter-planar distance is ca. 0.35 nm, corresponding to the (1 0 1) planes of anatase TiO_2. This further confirms that the crystalline structure of the TiO_2 nanorods coated on the titanate nanotubes is anatase phase.

3.2. S_{BET} and pore structures of the mesoporous titania nanorod/titanate nanotube composites

The nitrogen adsorption–desorption isotherms of the titanate nanotubes and the mesoporous titania nanorod/titanate nanotube composites (inset) are presented in Fig. 4. It can be seen that the as-prepared titanate nanotubes show the type IV isotherm with type H3 hysteresis loop according to BDDT classification [21], indicating the presence of mesopores (2–50 nm). Moreover, the observed hysteresis loop approaches $P/P_0 = 1$, suggesting the presence of macropores (>50 nm) [28]. As for the titania nanorod/titanate nanotube composites, the

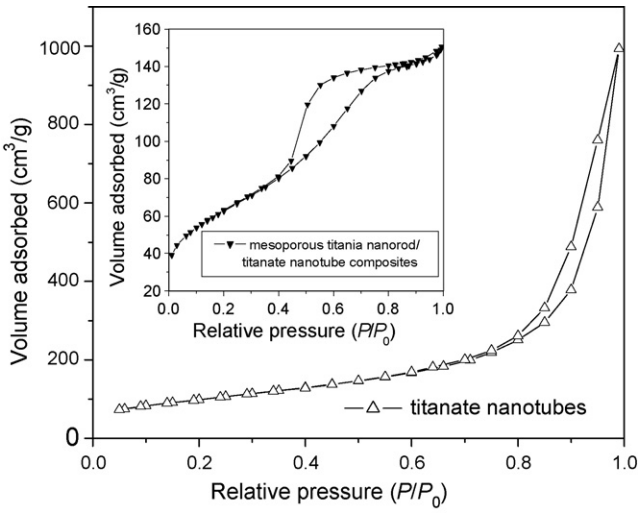

Fig. 4. Nitrogen adsorption–desorption isotherms of the titanate nanotubes and mesoporous titania nanorod/titanate nanotube composites (inset).

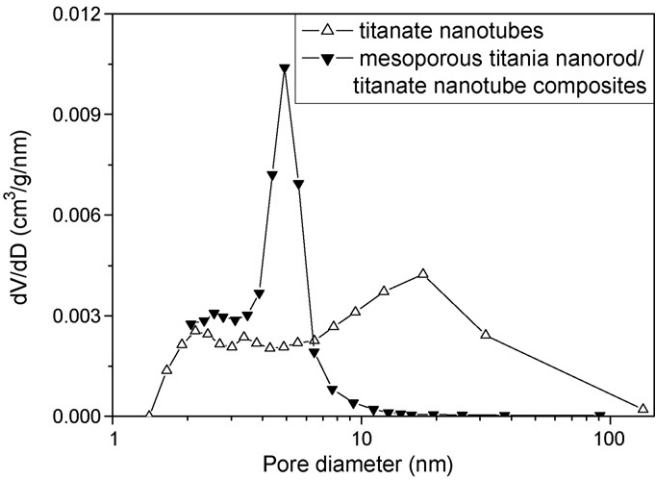

Fig. 5. Pore size distributions of the titanate nanotubes and the mesoporous titania nanorod/titanate nanotube composites.

adsorption–desorption isotherm of the sample is a combination of type I and IV (BDDT classification), with two very distinct regions of the low (0–0.2) and high (0.4–0.8) relative pressure. At the low relative pressure, the sample exhibits high adsorption, indicating the presence of micropores (type I). At high relative pressure (0.4–0.8), the curve exhibits an obvious hysteresis loop, indicating the presence of mesopores (type IV). Compared with the as-prepared titanate nanotubes, the titania nanorod/titanate nanotube composites shows almost no hysteresis loop at high relative pressure between 0.8 and 1.0, indicating the disappearance of the macropores (>50 nm).

Fig. 5 shows the corresponding pore size distributions of the as-prepared titanate nanotubes and the titania nanorod/titanate nanotube composites. Prior to the coating of the TiO_2 nanorods, the titanate nanotubes exhibit a wide pore size distribution (1.5 nm to more than 100 nm) with a maximum peak of 17.4 nm. This was in good agreement with the previous studies, though different TiO_2 sources were used as the precursors [28,29]. Considering the morphology of the nanotubes observed in Fig. 1, the smaller pores (<10 nm) may correspond to the pores inside the nanotubes and the diameters of these pores are equal to the inner diameter of the nanotubes, while the larger pores (10–100 nm) can be attributed to the aggregation of the nanotubes [28]. After the coating of the TiO_2 nanorods, the larger pores (10–100 nm), resulting from the aggregation of the titanate nanotubes, almost disappear completely due to the coating of the TiO_2 nanorods on the surface of the titanate nanotubes, leading to a narrow pore size distribution (~10 nm) with a maximum peak of 4.9 nm. Considering the morphologies of the titania nanorod/titanate nanotube composites (Fig. 3), the pores (<10 nm) in the sample can be attributed to two contributions. One is attributed to the aggregation of the TiO_2 nanoparticles in the TiO_2 nanorods and the other is ascribed to the pores within the titanate nanotubes. The textural parameters derived from the nitrogen adsorption–desorption isotherm data are summarized in Table 1. For comparison, the S_{BET} and pore structures of the P25 sample and the TiO_2 spherical aggregates are also tested under the identical conditions. When P25 transforms into the titanate

Table 1
BET specific surface area (S_{BET}) and pore parameters of the titanate nanotubes, TiO_2 spherical aggregates, P25, and the mesoporous titania nanorod/titanate nanotube composites

Samples	S_{BET} (m^2/g)	Pore volume (cm^3/g)	Pore size (nm)
Nanotubes	355.7	1.55	17.3
TiO_2 spheres	36.2	0.04	2.0
Composites	225.4	0.23	4.5
P25	49.3	0.09	8.3

nanotubes, there is a significant increase for S_{BET} from 49.3 to 355.7 m^2/g and for pore volume from 0.09 to 1.55 cm^3/g due to the formation of tube-like structures. After the coating of the TiO_2 nanorods on the surface of the titanate nanotubes, the S_{BET} and pore volumes decreased obviously, which are 225.4 m^2/g and 0.23 cm^3/g, respectively. However, it should be noted that the titania nanorod/titanate nanotube composites exhibit a greater S_{BET} and a higher pore volume than the precursor P25. The corresponding S_{BET} and the pore volume of the obtained samples are higher than that of P25 by a factor of about 4.6 and 2.6 times, respectively. The large specific surface area and high pore volume of the prepared samples are expected to result in a wider application in photocatalysis, selective adsorption, separation, sensing and as functional-filling materials in textile, paints, paper and cosmetics. Without the addition of titanate nanotubes, the S_{BET} and pore volume of the TiO_2 spherical aggregates decreased to 36.2 m^2/g and 0.04 cm^3/g, respectively. This can be attributed to the formation of solid spheres.

3.3. Photocatalytic activity

The photocatalytic activity of the mesoporous titania nanorod/titanate nanotube composites was evaluated by photocatalytic oxidation of acetone in air. Fig. 6 shows the comparison of apparent rate constants (k) of titanate nanotubes, TiO_2 spherical aggregates, mesoporous titania nanorod/titanate nanotube

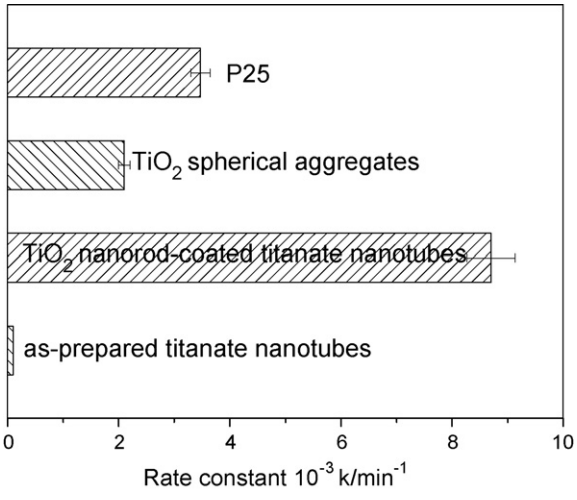

Fig. 6. The comparison of apparent rate constants of P25, titanate nanotubes, TiO_2 spherical aggregates and mesoporous titania nanorod/titanate nanotube composites.

composites and commercial photocatalyst P25. Prior to the coating of the anatase TiO_2 nanorods, the nanotubes almost showed no photocatalytic activity in spite of its high S_{BET} and pore volume. After the anatase TiO_2 nanorods were coated on the surface of the titanate nanotubes, the obtained sample showed highly photocatalytic activity. Compared with the as-prepared titanate nanotubes, the highly photocatalytic activity of the mesoporous titania nanorod/titanate nanotube composites could be ascribed to the formation of dispersed anatase TiO_2 nanorods on the surface of the titanate nanotubes. The k of the mesoporous titania nanorod/titanate nanotube composites reached ca. 8.7×10^{-3}, which exceeded that of P25 by a factor of about 2.5 times (Fig. 6). The k was determined to be 3.47×10^{-3} for Degussa P25, which is well known to have good photocatalytic activity. The superior activity of the mesoporous titania nanorod/titanate nanotube composites can be ascribed to their larger S_{BET} and higher pore volume (Table 1). Larger specific surface area allows more reactants to be absorbed on the surface of the photocatalyst, while higher pore volume results in a more rapid diffusion of various reactants and products during the photocatalytic reaction [24]. Of course, the smaller crystallite in the TiO_2 nanorods also contributed to the higher photocatalytic activity. As for the TiO_2 spherical sample, it showed a lower photocatalytic activity than the P25 owing to the aggregated structure, lower S_{BET} and pore volume.

The photocatalytic activities of the as-prepared titanate nanotubes and the mesoporous titania nanorod/titanate nanotube composites were further evaluated by photocatalytic discolorization of methyl orange aqueous solution. Fig. 7 shows the plots of absorbance (A) versus irradiation time (t) for the prepared samples. Illumination in the absence of photocatalysts did not result in the photocatalytic discolorization of methyl orange solution. It was found that the as-prepared nanotubes showed no photocatalytic activity, similar to the above result of photocatalytic oxidation of acetone in a gas phase. After the anatase

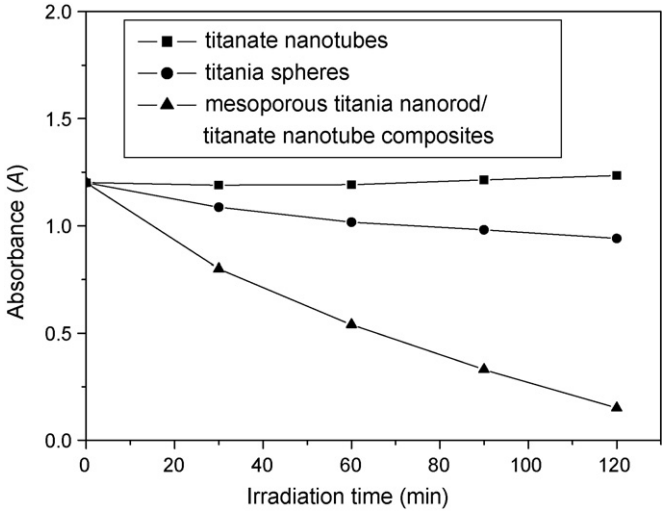

Fig. 7. Plots of absorbance (A) vs. irradiation time (t) for the titanate nanotubes, TiO_2 spherical aggregates, and the mesoporous titania nanorod/titanate nanotube composites. Absorbance (A) in the Y-axis is proportional to the concentration (c).

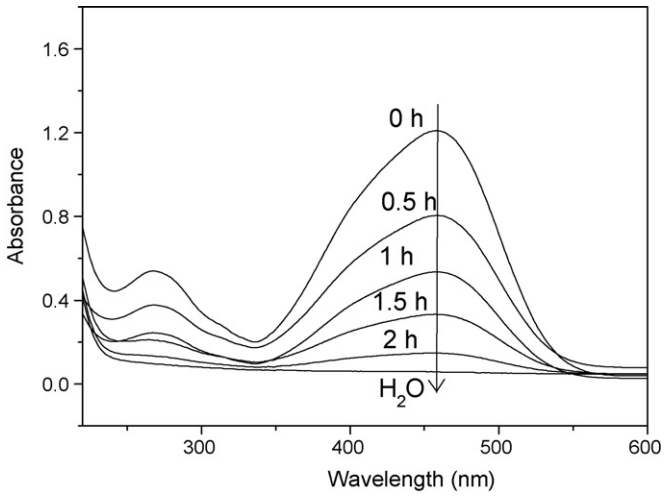

Fig. 8. Change of absorption spectra of the methyl orange aqueous solution during its photocatalytic discolorization using the mesoporous titania nanorod/titanate nanotube composites as the photocatalyst.

TiO_2 nanorods were uniformly coated on the surface of the titanate nanotubes, the obtained sample showed highly photocatalytic activity and the concentration of the methyl orange decreased rapidly with increasing UV irradiation time. Fig. 8 shows the change of absorption spectra of the methyl orange aqueous solution during its photocatalytic discolorization using the mesoporous titania nanorod/titanate nanotube composites as the photocatalyst. For comparison, the absorption spectrum of the distilled water was also measured under the same conditions. It could be seen that the absorption peak gradually decreased with increasing UV irradiation time. After UV irradiation for ca. 2 h, the absorption peak of the methyl orange aqueous solution was very weak. Moreover, experimental observation indicated that the color of the methyl orange aqueous solution changed from orange to near no color after UV irradiation for ca. 2 h, indicating a nearly complete degradation of methyl orange. When the P25 powder was used as the photocatalyst for the degradation of methyl orange, similar discolorization phenomenon in the aqueous solution was also found. However, the P25 powder could not be readily separated from the reaction system after photocatalytic reaction. In this investigation, the mesoporous titania nanorod/titanate nanotube composites were prepared and their length was usually in the range of several hundreds of nanometers (Fig. 3). Compared with the nanosized powder photocatalysts such as P25 photocatalyst, the mesoporous titania nanorod/titanate nanotube composites could be readily separated from a slurry system after photocatalytic reaction owing to their long structure. Though the prepared TiO_2 microspheres could also be readily separated from a slurry system, the TiO_2 spherical samples showed a low photocatalytic activity. Therefore, we think that the titania nanorod/titanate nanotube composites are one of the ideal and novel photocatalysts for the applications of anatase nanoparticles in the environmental purification and water treatment and this investigation may provide new insights into preparing novel highly photoactive catalysts to avoid the disadvantages of the powder and thin film photocatalysts. Therefore, the prepared mesoporous tita-

nia nanorod/titanate nanotube composite photocatalysts with highly photocatalytic activity may be suitable for the application of anatase photocatalysts at industrial scale, which has been seriously impeded by the high cost for separating the catalyst nanocrystals [30].

4. Conclusions

Mesoporous titania nanorod/titanate nanotube composites were successfully prepared using TiF_4 and H_3BO_3 as the precursors. It was found that the obtained mesoporous titania nanorod/titanate nanotube composites showed a larger specific surface area and a higher pore volume, which is higher than that of P25 by a factor of about 4.6 and 2.6 times, respectively, leading to an obvious enhancement of the photocatalytic activity for the photocatalytic oxidation of acetone. Moreover, the mesoporous titania nanorod/titanate nanotube composites, which could be readily separated after photocatalytic reaction, exhibited highly photocatalytic activity for the degradation of methyl orange aqueous solution.

Acknowledgements

This work was partially supported by the National Natural Science Foundation of China (20473059 and 50625208). This work was also financially supported by the Key Research Project of Chinese Ministry of Education (No. 106114) and Program for Changjiang Scholars and Innovative Research Team in University (PCSIRT, No. IRT0547), Ministry of Education, China.

References

[1] M.R. Hoffmann, S.T. Martin, W. Choi, D.W. Bahnemann, Environmental applications of semiconductor photocatalysis, Chem. Rev. 95 (1995) 69.
[2] J.C. Zhao, T.X. Wu, K.Q. Wu, K. Oikawa, H. Hidaka, N. Serpone, Photoassisted degradation of dye pollutants. 3. Degradation of the cationic dye rhodamine B in aqueous anionic surfactant/TiO_2 dispersions under visible light irradiation: evidence for the need of substrate adsorption on TiO_2 particles, Environ. Sci. Technol. 32 (1998) 2394.
[3] J.G. Yu, H.G. Yu, B. Cheng, X.J. Zhao, J.C. Yu, W.K. Ho, The effect of calcination temperature on the surface microstructure and photocatalytic activity of TiO_2 thin films prepared by liquid phase deposition, J. Phys. Chem. B 107 (2003) 13871.
[4] F.B. Li, X.Z. Li, M.F. Hou, Photocatalytic degradation of 2-mercaptobenzothiazole in aqueous La^{3+}–TiO_2 suspension for odor control, Appl. Catal. B 48 (2004) 185.
[5] J.G. Yu, X.J. Zhao, Q.N. Zhao, Effect of surface structure on photocatalytic activity of TiO_2 thin films prepared by sol–gel method, Thin Solid films 379 (2000) 7.
[6] H.G. Yu, S.C. Lee, J.G. Yu, C.H. Ao, Photocatalytic activity of dispersed TiO_2 particles deposited on glass fibers, J. Mol. Catal. A 246 (2006) 206.
[7] J.C. Yu, J. Lin, D. Lo, S.K. Lam, Influence of thermal treatment on the adsorption of oxygen and photocatalytic activity of TiO_2, Langmuir 16 (2000) 7304.
[8] J.G. Yu, J.C. Yu, M.K.P. Leung, W.K. Ho, B. Cheng, X.J. Zhao, J.C. Zhao, Effects of acidic and basic hydrolysis catalysts on the photocatalytic activity and microstructures of bimodal mesoporous titania, J. Catal. 217 (2003) 69.
[9] D.V. Bavykin, A.A. Lapkin, P.K. Plucinski, J.M. Friedrich, F.C. Walsh, TiO_2 nanotube-supported ruthenium(III) hydrated oxide: a highly active catalyst for selective oxidation of alcohols by oxygen, J. Catal. 235 (2005) 10.
[10] J.C. Yu, J.G. Yu, J.C. Zhao, Enhanced photocatalytic activity of mesoporous and ordinary TiO_2 thin films by sulfuric acid treatment, Appl. Catal. B 36 (2002) 31.
[11] H. Pizem, C.N. Sukenik, U. Sampathkumaran, A.K. McIlwain, M.R. De Guire, Effects of substrate surface functionality on solution-deposited titania films, Chem. Mater. 14 (2002) 2476.
[12] Y. Masuda, S. Ieda, K. Koumoto, Site-selective deposition of anatase TiO_2 in an aqueous solution using a seed layer, Langmuir 19 (2003) 4415.
[13] S. Deki, Y. Aoi, O. Hiroi, A. Kajinami, Titanium (IV) oxide thin films prepared from aqueous solution, Chem. Lett. 6 (1996) 433.
[14] T. Kasuga, M. Hiramatsu, A. Hoson, T. Sekino, K. Niihara, Formation of titanium oxide nanotube, Langmuir 14 (1998) 3160.
[15] T. Kasuga, M. Hiramatsu, A. Hoson, T. Sekino, K. Niihara, Titania nanotubes prepared by chemical processing, Adv. Mater. 11 (1999) 1307.
[16] Q. Chen, W.Z. Zhou, G.H. Du, L.M. Peng, Trititanate nanotubes made via a single alkali treatment, Adv. Mater. 14 (2002) 1208.
[17] G.H. Du, Q. Chen, R.C. Che, Z.Y. Yuan, L.P. Peng, Preparation, structure analysis of titanium oxide nanotubes, Appl. Phys. Lett. 79 (2001) 3702.
[18] Z.Y. Yuan, W. Zhou, B.L. Su, Hierarchical interlinked structure of titanium oxide nanofibers, Chem. Commun. (2002) 1202.
[19] S.M. Liu, L.M. Gan, L.H. Liu, W.D. Zhang, H.C. Zeng, Synthesis of single-crystalline TiO_2 nanotubes, Chem. Mater. 14 (2002) 1391.
[20] X.M. Sun, Y.D. Li, Synthesis and characterization of ion-exchangeable titanate nanotubes, Chem. Eur. J. 9 (2003) 2229.
[21] K.S.W. Sing, D.H. Everett, R.A.W. Haul, L. Moscou, R.A. Pierotti, J. Rouquerol, T. Siemieniewska, Reporting physisorption data for gas/solid systems with special reference to the determination of surface area and porosity, Pure Appl. Chem. 57 (1985) 603.
[22] M.E. Zorn, D.T. Tompkins, W.A. Zeltner, M.A. Anderson, Photocatalytic oxidation of acetone vapor on TiO_2/ZrO_2 thin films, Appl. Catal. B 23 (1999) 1.
[23] J.G. Yu, H.G. Yu, B. Cheng, X.J. Zhao, Q.J. Zhang, Preparation, photocatalytic activity of mesoporous anatase TiO_2 nanofibers by a hydrothermal method, J. Photochem. Photobiol. A 182 (2006) 121.
[24] J.G. Yu, H.G. Yu, B. Cheng, M.H. Zhou, X.J. Zhao, Enhanced photocatalytic activity of TiO_2 powder (P25) by hydrothermal treatment, J. Mol. Catal. A 253 (2006) 112.
[25] R. Ma, Y. Bando, T. Sasaki, Nanotubes of lepidocrocite titanates, Chem. Phys. Lett. 380 (2003) 577.
[26] H.G. Yu, J.G. Yu, B. Cheng, M.H. Zhou, Effects of hydrothermal post-treatment on microstructures and morphology of titanate nanoribbons, J. Solid State Chem. 179 (2006) 349.
[27] J. Canales, P.G. Bruce, TiO_2-B nanowires, Angew. Chem. Int. Ed. 43 (2004) 2286.
[28] D.V. Bavykin, V.N. Parmon, A.A. Lapkin, F.C. Walsh, The effect of hydrothermal conditions on the mesoporous structure of TiO_2 nanotubes, J. Mater. Chem. 14 (2004) 3370.
[29] C.C. Tsai, H. Teng, Regulation of the physical characteristics of titania nanotube aggregates synthesized from hydrothermal treatment, Chem. Mater. 16 (2004) 4352.
[30] H. Zhu, X. Gao, Y. Lan, D. Song, Y. Xi, J. Zhao, Hydrogen titanate nanofibers covered with anatase nanocrystals: a delicate structure achieved by the wet chemistry reaction of the titanate nanofibers, J. Am. Chem. Soc. 126 (2004) 8380.